Chapter 2
An Advanced Constitutive Law in Multiphase Flow Model for Simulations in Compressible Media

C.H. Tsai and G.T. Yeh

Abstract The purpose of this investigation is to implement a new constitutive law of saturation–capillary pressure into a fractional flow-based multiphase flow model to simulate compressible subsurface flow problems. Using the new constitutive law to describe the saturation–capillary pressure relations alleviates an undue constraint on pressure distributions inherent in a widely used law. This makes the present model able to include all possible solutions of pressure distributions in subsurface flow modeling. Finite element methods (FEM) are used to discretize the three governing equations for three primary variables—saturation of water, saturation of total liquid, and total pressure. Four examples with different pressure distributions are presented to show the feasibility and advantage of using the new constitutive law. The results verify the feasibility and capability of the present model for subsurface flow systems to cover all possible pressure distributions.

2.1 Introduction

In general, it is challenging to simultaneously measure degrees of saturation and capillary pressures in subsurface flow systems. Therefore, a complete and possible analytic model of constitutive law is essential for the multiple-phase flow simulation. A widely used saturation–capillary pressure relationship for three-phase flow was proposed by Parker et al. (1987a). Since the closed-form expression of the saturation–capillary pressure relationship is quite simple, the model has been widely

C.H Tsai (✉) • G.T. Yeh
Graduate Institute of Applied Geology, National Central University, Jhongli City, Taoyuan 32001, Taiwan
e-mail: f92521314@ntu.edu.tw; gyeh@ncu.edu.tw

P.K. Mishra and K.L. Kuhlman (eds.), *Advances in Hydrogeology*,
DOI 10.1007/978-1-4614-6479-2_2,

used in systems of two- and three-phase flows (e.g., Parker and Lenhard 1987b; Kaluarachchi and Parker 1989; Celia and Binning 1992; White and Oostrom 1996; Guarnaccia and Pinder 1997; Binning and Celia 1999; Suk and Yeh 2007; Suk and Yeh 2008; Khoei and Mohammadnejad 2011).

An undue constraint in Parker et al.'s model, the product of the scaling factor and capillary pressure between nonaqueous phase liquid (NAPL) and air must be less than or equal to that between water and NAPL (Tsai and Yeh 2012). This constraint has not been supported theoretically or experimentally. To our knowledge, this constraint has not been discussed in the literature. Moreover, due to the widespread use of Parker et al.'s model, many available multiphase flow simulations may be incomplete. For problems with pressure distributions that do not satisfy the constraint, negative saturations might be obtained and thus leads the simulations stymied using fractional flow-based approaches (e.g., Binning and Celia 1999; Guarnaccia and Pinder 1997; Suk and Yeh 2007; Suk and Yeh 2008). Possible solutions will be excluded without physical justifications using the variable-switch technique (White and Oostrom 1996) in pressure-based approaches (e.g., Kaluarachchi and Parker 1989; Celia and Binning 1992), i.e., the variable-switch algorithm implemented in those models would exclude some prescribed conditions due to the use of Parker's constitutive law. For example, simulations with those models will exclude initial and boundary conditions that might otherwise be possible.

A new constitutive relation between the degree of saturation and capillary pressure was proposed to overcome the undue constraint (Tsai and Yeh 2012). The main objective of this chapter is to implement the new constitutive law in a compressible multiple-phase flow model using fractional flow-based approaches. The implementation yields solutions even when the initial and boundary pressure distribution does not satisfy the constraint. Had it been implemented in a pressure-based approach numerical model, it will not have to exclude some possible solutions.

In multiphase flow simulations, the fractional flow-based approach is widely used due to two advantages. First, the primary variables in the fractional flow-based approach are degrees of saturation and total pressure. Therefore, the change of phase configuration, phase appearance, and phase disappearance are automated. For example, the number of simulated phases in a three-phase flow problem can degenerate from three to two or one and conversely extend from one to two or three (Suk and Yeh 2008). Second, for incompressible three-phase flow problems, one solves an elliptic-type equation for total pressure and two hyperbolically dominant types of transport equations for degrees of saturation with the fractional flow-based approach, instead of solving three strongly coupled nonlinear mixed hyperbolic and parabolic-type equations with the pressure-based approach. Although this requires an extra task of iterating boundary conditions, only two or three iterations will suffice (Suk and Yeh 2008). From the viewpoint of numerical computation, the fractional flow-based approach is quite efficient (Suk and Yeh 2008).

In this investigation, the fractional flow-based approach is employed to simulate compressible multiphase flow problems. The primary variables of the three

governing equations are the saturation of water, the saturation of total liquid, and the total pressure. Because the compressibility of each flow phase is considered, we simulate one parabolic-dominant equation for total pressure and two hyperbolic-dominant equations for degrees of saturation. Three governing equations and compressibility are presented in Sect. 2.2. In Sect. 2.3, both Parker et al.'s and Tsai and Yeh's constitutive models are presented and discussions are made on why the former results in the undue constraint while the latter does not. The numerical discretizations with FEM for three governing equations are given in Appendix A. The standard Galerkin FEM is used to discretize the governing equation for total pressure, and either the standard Galerkin FEM or the upstream FEM are used to discretize two equations for saturations of water and total liquid. The resulting matrix is solved with the Bi-CGSTAB (vant der Vorst 1992). In Sect. 2.4, four numerical examples are used to verify the feasibility and capability of the present numerical model to include all possible conditions that are prescribed. The conclusions are made in Sect. 2.5.

2.2 Problem Formulations

The present multiphase flow model is assumed to consist of a compressible media and three compressible fluid phases consisting of water, NAPL, and air The porosity is assumed constant in the simulation. Each phase is assumed to have an average property, since each phase contains one component in this investigation. These assumptions do not alter the key points to be addressed in this chapter. However, a model without these assumptions is under development to make it more applicable to real-world problems.

2.2.1 Governing Equations

The mass conservation equation for each phase in porous media is given as follows (Yeh et al. 2010):

$$\begin{aligned}
&\frac{\partial\left(\phi\rho_i S_i\right)}{\partial t}+\nabla\cdot\left(\mathbf{M}_i\right)+\nabla\cdot\left(\rho_i\phi S_i\mathbf{V}_s\right)=Q_i,\quad i=1,2,3.\\
&\frac{\partial\rho_s\left(1-\phi\right)}{\partial t}+\nabla\cdot\left[\rho_s\left(1-\phi\right)\mathbf{V}_s\right]=0,
\end{aligned}\tag{2.1}$$

in which

$$\mathbf{M}_i=\rho_i\mathbf{V}_i=-\frac{\rho_i k_{ri}\mathbf{k}}{\mu_i}\cdot\left(\nabla P_i+\rho_i g\nabla z\right),\quad i=1,2,3,\tag{2.2}$$

where i is the subscript index relating to Phase 1 for water, Phase 2 for NAPL and Phase 3 for air; ϕ is the effective porosity; t is the time, [T]; ρ_i is the density for phase i, $\left[\mathrm{M/L^3}\right]$; ρ_s is the density for solid phase, $\left[\mathrm{M/L^3}\right]$; Q_i is the source or sink for phase i, $\left[\mathrm{M/\left(L^3T\right)}\right]$; S_i is the degree of saturation for phase i;M_i is the Darcy's mass flux, $\left[\mathrm{M/\left(L^2T\right)}\right]$; $\mathbf{v}_i$ is the Darcy's velocity for phase i, [L/T]; $\mathbf{v}_s$ is the velocity for solid phase, [L/T]; $\mathbf{k}$ is the intrinsic permeability tensor, $\left[\mathrm{L^2}\right]$; k_{ri} is the relative permeability for phase i; μ_i is the dynamic viscosity for phase i, [M/L/T]; P_i is the pressure for phase i $\left[\mathrm{M/L/T^2}\right]$; g is the gravitational constant $\left[\mathrm{L/T^2}\right]$; and z is the elevation, [L].

With some manipulations, Eq (2.1) becomes

$$\phi\frac{\partial\left(\rho_i S_i\right)}{\partial t}+\rho_i S_i\left(\nabla\cdot\mathbf{V}_s\right)+\nabla\cdot\left(\mathbf{M}_i\right)=Q_i,\quad i=1,2,3. \tag{2.3}$$

With small and vertical displacement (Yeh et al. 2010), Eq (2.3) becomes

$$\phi\frac{\partial\left(\rho_i S_i\right)}{\partial t}+\rho_i S_i\left(\alpha_p\sum_{j=1}^{3}\frac{\partial\left(S_j P_j\right)}{\partial t}\right)+\nabla\cdot\left(\mathbf{M}_i\right)=Q_i,\quad i=1,2,3, \tag{2.4}$$

where α_p is the compressibility parameter of the medium, $\left[\left(\mathrm{T^2L}\right)/\mathrm{M}\right]$

Substituting Eq (2.2) into Eq (2.4) and summing the resulting equations over three phases one obtains the following equation for the total pressure:

$$\begin{aligned}&C_{pt}\frac{\partial P_t}{\partial t}+C_{s1}\frac{\partial S_1}{\partial t}+C_{st}\frac{\partial S_t}{\partial t}-\nabla\cdot\boldsymbol{\kappa}\cdot\left(\nabla P_t+\bar{\rho}g\nabla z\right)=Q_t\\&-\left[\left(\rho_1-\rho_2\right)S_1+\left(\rho_2-\rho_3\right)S_t+\rho_3\right]\left[\alpha_p\left(\left(P_1-P_2\right)S_1+\left(P_2-P_3\right)S_t+P_3\right)\right],\end{aligned} \tag{2.5}$$

in which

$$\boldsymbol{\kappa}=\mathbf{k}\left(\rho_1 k_{r1}/\mu_1+\rho_2 k_{r2}/\mu_2+\rho_3 k_{r3}/\mu_3\right), \tag{2.6}$$

$$\bar{\rho}=\kappa_1\rho_1+\kappa_2\rho_2+\kappa_3\rho_3, \tag{2.7}$$

$$\kappa_i=\rho_i k_{ri}/\mu_i/\sum_{j=1}^{3}\rho_j k_{rj}/\mu_j,\quad \text{for}\quad i=1,2\ \textit{and}\ 3, \tag{2.8}$$

$$\begin{aligned}P_t=&\frac{P_1+P_2+P_3}{3}\\&+\frac{1}{3}\left(\int_0^{P_{C12}}\left(\kappa_1-\kappa_2\right)\mathrm{d}\eta+\int_0^{P_{C13}}\left(\kappa_1-\kappa_3\right)\mathrm{d}\eta+\int_0^{P_{C23}}\left(\kappa_2-\kappa_3\right)\mathrm{d}\eta\right),\end{aligned} \tag{2.9}$$

$$C_{pt} = \phi S_1 \frac{\partial \rho_1}{\partial P_1} + \phi S_2 \frac{\partial \rho_2}{\partial P_2} + \phi S_3 \frac{\partial \rho_3}{\partial P_3} + (\rho_1 S_1 + \rho_2 S_2 + \rho_3 S_3)\,\alpha_p, \tag{2.10}$$

$$\begin{aligned} C_{s1} = {} & \phi S_1 \frac{\partial \rho_1}{\partial P_1}(1-\kappa_1)\frac{\mathrm{d}P_{C12}}{\mathrm{d}S_1} - \phi S_2 \frac{\partial \rho_2}{\partial P_2}\kappa_1 \frac{\mathrm{d}P_{C12}}{\mathrm{d}S_1} \\ & -\phi S_3 \frac{\partial \rho_3}{\partial P_3}\kappa_1 \frac{\mathrm{d}P_{C12}}{\mathrm{d}S_1} + \phi(\rho_1 - \rho_2) \\ & + (\rho_1 S_1 + \rho_2 S_2 + \rho_3 S_3)\,\alpha_p \left[P_{C12} + (S_1 - \kappa_1)\frac{\mathrm{d}P_{C12}}{\mathrm{d}S_1}\right], \end{aligned} \tag{2.11}$$

$$\begin{aligned} C_{st} = {} & \varphi S_1 \frac{\partial \rho_1}{\partial P_1}\kappa_3 \frac{\mathrm{d}P_{C23}}{\mathrm{d}S_t} + \phi S_2 \frac{\partial \rho_2}{\partial P_2}\kappa_3 \frac{\mathrm{d}P_{C23}}{\mathrm{d}S_t} \\ & -\phi S_3 \frac{\partial \rho_3}{\partial P_3}(1-\kappa_3)\frac{\mathrm{d}P_{C23}}{\mathrm{d}S_t} + \phi(\rho_2 - \rho_3) \\ & + (\rho_1 S_1 + \rho_2 S_2 + \rho_3 S_3)\,\alpha_p \left[P_{C23} + (S_t - 1 + \kappa_3)\frac{\mathrm{d}P_{C23}}{\mathrm{d}S_t}\right] \end{aligned} \tag{2.12}$$

$$Q_t = Q_1 + Q_2 + Q_3 \tag{2.13}$$

$$S_t = S_1 + S_2 = 1 - S_3 \tag{2.14}$$

where $\boldsymbol{\kappa}$ is the total mobility, [T]; $\overline{\rho}$ is the mobility weighted average fluid density, $\left[\mathrm{M/L}^3\right]$; κ_1, κ_2, and κ_3 are, respectively, the fractional mobility for water, NAPL and air; P_t is the total pressure, $\left[\mathrm{M/T}^2\mathrm{/L}\right]$; S_1, S_2, S_3, and S_t are, respectively the saturation of water, NAPL, air, and total liquid; $P_{C12} \equiv P_1 - P_2$ is the capillary pressure of waterNAPL; $P_{C13} \equiv P_1 - P_3 = -P_{C31}$ is the capillary pressure of waterair; and $P_{C23} \equiv P_2 - P_3$ is the capillary pressure of NAPLair Substituting Eq (2.2) with Phases 1 and 3 into Eq (2.4) and with some manipulations, the transport equations for the saturation of water S_1 and the saturation of total liquid S_t, respectively, are given as

$$\begin{aligned} & \left(\phi S_1 \frac{\partial \rho_1}{\partial P_1} - \kappa_1 C_{pt} + \rho_1 S_1 \alpha_p\right)\frac{\partial P_t}{\partial t} + \begin{pmatrix} \phi S_1 \frac{\partial \rho_1}{\partial P_1}(1-\kappa_1)\frac{\mathrm{d}P_{C12}}{\mathrm{d}S_1} + \rho_1 \phi - \kappa_1 C_{s1} \\ + \rho_1 S_1 \alpha_p \left[P_{C12} + (S_1 - \kappa_1)\frac{\mathrm{d}P_{C12}}{\mathrm{d}S_1}\right]\frac{\partial S_1}{\partial t} \end{pmatrix} \\ & + \left(\phi S_1 \frac{\partial \rho_1}{\partial P_1}\kappa_3 \frac{\mathrm{d}P_{C23}}{\mathrm{d}S_t} - \kappa_1 C_{st} + \rho_1 S_1 \alpha_p \left[P_{C23} + (S_t - 1 + \kappa_3)\frac{\mathrm{d}P_{C23}}{\mathrm{d}S_t}\right]\right)\frac{\partial S_t}{\partial t} \\ & + \mathbf{M}_t \cdot \frac{\mathrm{d}\kappa_1}{\mathrm{d}S_1}\nabla S_1 + \mathbf{M}_t \cdot \frac{\mathrm{d}\kappa_1}{\mathrm{d}S_t}\nabla S_t \\ & = -\kappa_1 Q_t + \nabla \cdot \kappa_1 \boldsymbol{\kappa} \cdot \left((1-\kappa_1)\frac{\mathrm{d}P_{C12}}{\mathrm{d}S_1}\nabla S_1 + \kappa_3 \frac{\mathrm{d}P_{C23}}{\mathrm{d}S_t}\nabla S_t + (\rho_1 - \overline{\rho})\,g\nabla z\right) + Q_1 \end{aligned} \tag{2.15}$$

and

$$
\begin{aligned}
&-\left(\phi S_3\frac{\partial\rho_3}{\partial P_3}-\kappa_3 C_{pt}+\rho_3 S_3\alpha_p\right)\frac{\partial P_t}{\partial t}+\left(\begin{array}{l}\phi S_3\dfrac{\partial\rho_3}{\partial P_3}\kappa_1\dfrac{\mathrm{d}P_{C12}}{\mathrm{d}S_1}+\kappa_3 C_{s1}\\ -\rho_3 S_3\alpha_p\left[P_{C12}+(S_1-\kappa_1)\frac{\mathrm{d}P_{C12}}{\mathrm{d}S_1}\right]\end{array}\right)\frac{\partial S_1}{\partial t}\\
&+\left(\phi S_3\frac{\partial\rho_3}{\partial P_3}(1-\kappa_3)\frac{\mathrm{d}P_{C23}}{\mathrm{d}S_t}+\kappa_3 C_{st}+\rho_3\phi-\rho_3 S_3\alpha_p\right.\\
&\left.\times\left[P_{C23}+(S_t-1+\kappa_3)\frac{\mathrm{d}P_{C23}}{\mathrm{d}S_t}\right]\right)\frac{\partial S_t}{\partial t}\\
&-\mathbf{M}_t\cdot\frac{\mathrm{d}\kappa_3}{\mathrm{d}S_1}\nabla S_1-\mathbf{M}_t\cdot\frac{\mathrm{d}\kappa_3}{\mathrm{d}S_t}\nabla S_t\\
&=+\kappa_3 Q_t+\nabla\cdot\kappa_3\boldsymbol{\kappa}\cdot\left(\kappa_1\frac{\mathrm{d}P_{C12}}{\mathrm{d}S_1}\nabla S_1+(1-\kappa_3)\frac{\mathrm{d}P_{C23}}{\mathrm{d}S_t}\nabla S_t-(\rho_3-\overline{\rho})\,g\nabla z\right)-Q_3,
\end{aligned}
\tag{2.16}
$$

in which

$$\mathbf{M}_t=\mathbf{M}_1+\mathbf{M}_2+\mathbf{M}_3, \tag{2.17}$$

where M_i is the total mass flux, $\left[\mathrm{M}/\left(\mathrm{L}^2\mathrm{T}\right)\right]$

These three equations must be supplemented with the constitutive laws for the relative permeability versus degree of saturation and the degree of saturation versus capillary pressure.

2.2.2 Compressibility of Three Fluid Phases

The equations of state for water and NAPL are individually given as

$$\frac{\partial\rho_1}{\partial P_1}=\beta_1\rho_1^0, \tag{2.18}$$

$$\frac{\partial\rho_2}{\partial P_2}=\beta_2\rho_2^0, \tag{2.19}$$

where β_1 and β_2 are compressibility of water and NAPL, respectively, $\left[\mathrm{T}^2\mathrm{L}/\mathrm{M}\right]$ and ρ_1^0 and ρ_2^0 are the reference densities of water and NAPL, respectively, $\left[\mathrm{M}/\mathrm{L}^3\right]$. In addition, the compressibility of air is given as

$$\frac{\partial\rho_3}{\partial P_3}=\frac{\mathrm{M}}{\mathrm{RT}} \tag{2.20}$$

where M is the mole weight of air, $\left[\mathrm{Mmole}^{-1}\right]$; R is the gas constant, $\left[\mathrm{ML}^2\mathrm{T}^{-2}\mathrm{mole}^{-1}\mathrm{K}^{-1}\right]$; and T is the absolute temperature, [K].

2.3 The Constitutive Laws

The constitutive law relating the capillary pressure to the degree of saturation can be derived based on the fundamental Young–Laplace equation (Laplace 1806). The equation relating the relative hydraulic conductivity to the degree of saturation can be derived based on the theory proposed by Mualem (1976).

2.3.1 Parker et al.'s Model for Three-Phase Fluids

Parker et al.'s three-phase model is an extension of the renown two-phase model proposed by van Genuchten (1980).

2.3.1.1 The Relations of Saturation and Capillary Pressure

Based on the assumption that fluid wettability follows the sequence water → NAPL → air, Parker et al. (1987a) extended the saturation–capillary pressure relationship (van Genuchten, 1980) from two-phase fluids to three-phase fluids. With the definition of the accumulated liquid saturation, a straightforward extension of van Genuchten's model results in the following relationship (Parker et al. 1987a):

$$\begin{aligned} &S_1 = 1 \text{ for } h_{C21} \le 0 \quad \text{and} \quad S_1 = \left[1 + (\alpha_{21} h_{C21})^n\right]^{-m} \text{ for } h_{C21} > 0; \\ &S_t = 1 \text{ for } h_{C32} \le 0 \quad \text{and} \quad S_t = \left[1 + (\alpha_{32} h_{C32})^n\right]^{-m} \text{ for } h_{C32} > 0; \\ &S_2 = S_t - S_1; \quad \text{and} \quad S_3 = 1 - S_t \end{aligned} \tag{2.21}$$

in which

$$m = 1 - 1/n, \tag{2.22}$$

where m and n are the curve shape parameters; α_{32} is the scaling factor of capillary pressure head between air and NAPL, [1/L]; α_{21} is the scaling factor of capillary pressure head between NAPL and water [1/L]; h_{C32} is the capillary pressure head between air and NAPL, [L]; and h_{C21} is the capillary pressure head between NAPL and water [L].

From Eq. (2.21), it is seen that as the degree of saturation increases, the scaled capillary pressure decreases. According to the definition of the total liquid saturation, S_t is greater than or equal to S_1. Thus, one can conclude that capillary pressure between NAPL and air must be less than or equal to that between water and NAPL as

$$(\alpha_{32} h_{C32}) \le (\alpha_{21} h_{C21}). \tag{2.23}$$

Obviously, Parker et al.'s model implies that the closed-form expression in Eq. (2.21) is workable only if the products of the scaling factor and capillary pressure head, $(\alpha_{32}h_{C32})$ and $(\alpha_{21}h_{C21})$, satisfy the constraint in Eq. (2.23). This constraint seems to have little physical relevance. In other words, some possible distributions of pressure head among phase fluids are excluded due to the constitutive law by Parker et al., not due to physical justifications. To our knowledge, no literature exists confirming the validity of Inequality (2.23).

2.3.1.2 The Relations of Relative Permeability and Saturation

In Parker et al.'s model, the relative permeability as a function of the degree of saturation is proposed by Parker et al. (1987a), which is the modified van Genuchten's model of two-phase flow (van Genuchten 1980):

$$k_{r1} = \bar{S}_1^{1/2}\left[1-\left(1-\bar{S}_1^{1/m}\right)^m\right]^2, \tag{2.24}$$

$$k_{r2} = \left(\bar{S}_t-\bar{S}_1\right)^{1/2}\left[\left(1-\bar{S}_1^{1/m}\right)^m-\left(1-\bar{S}_t^{1/m}\right)^m\right]^2, \tag{2.25}$$

$$k_{r3} = \left(1-\bar{S}_t\right)^{1/2}\left(1-\bar{S}_t^{1/m}\right)^{2m}, \tag{2.26}$$

in which

$$\bar{S}_1 = (S_1-S_{1r})/(1-S_{1r}), \tag{2.27}$$

$$\bar{S}_t = (S_1+S_2-S_{1r})/(1-S_{1r}), \tag{2.28}$$

where $\bar{S}_1$ is the effective degree of saturation for water, S_{1r} is the irreducible saturation of water and $\bar{S}_t$ is the effective degree of saturation for total liquid.

2.3.2 Tsai and Yeh's Model for L-Phase Fluids

Because of the undue constraint in Parker et al.'s model, a new model was proposed to alleviate this constraint. The model was derived based on two hypotheses (Yeh and Tsai 2011): (1) the capillary pressure function is homogeneous, i.e., it is independent of phases and (2) the capillary pressure function is a function of the accumulated degrees of saturation of two neighboring phases only, i.e. the capillary pressure function is of degree 1. Then, it was postulated that the capillary pressure is a unique function of a single variable defined as the ratio of the two total accumulated degree of saturation (Tsai and Yeh 2012).

2.3.2.1 The Relations of Saturation and Capillary Pressure

Specifically, analogous to the van Genuchen's model (van Genuchten 1980),the model proposed by Tsai and Yeh (2012) is given as follows:

$$\frac{S_{t,i}}{S_{t,i+1}} \equiv \Theta_i = \begin{cases} 1 \text{ for } h_{Ci+1,i} \leq 0 \\ \left[1 + (\alpha_{i+1,i} h_{Ci+1,i})^n\right]^{-m} \text{ for } h_{Ci+1,i} > 0, \end{cases}$$
$$i = 1, 2, \ldots, L-1; \Theta_0 = 0; \Theta_{\mathrm{L}} = 1, \tag{2.29}$$

where $S_{t,i}$ is the total degree of saturation accumulated up to the $i-$th phase, $S_{t,i+1}$ is the total degree of saturation accumulated up to the $(i+1)-$th phase, Θ_i is the ratio of the total accumulated degree of saturation of the relatively wetting phase ($i-$th phase) to that of the relatively non-wetting phase ($(i+1)-$th phase), $\alpha_{i+1,i}$ is the scaling factor between the $(i+1)-$phase and $i-$phase and $h_{Ci+1,i} \equiv h_{i+1} - h_i$ is the capillary pressure head between the $(i+1)-$phase and $i-$phase, [L].

For three-phase flow (water-NAPL-air) problems, the expression of saturation–capillary pressure head relationship (2.29) is given as follows:

$$\Theta_1 \equiv \frac{S_1}{S_t} = 1 \text{ for } h_{C21} \leq 0 \quad \text{and} \quad \Theta_1 \equiv \frac{S_1}{S_t} = \left[1 + (\alpha_{21} h_{C21})^n\right]^{-m} \text{ for } h_{C21} > 0;$$
$$\Theta_2 \equiv \frac{S_t}{1} = 1 \text{ for } h_{C32} \leq 0 \quad \text{and} \quad \Theta_2 \equiv \frac{S_t}{1} = \left[1 + (\alpha_{32} h_{C32})^n\right]^{-m} \text{ for } h_{C32} > 0;$$
$$S_2 = S_t - S_1; \text{ and } S_3 = 1 - S_t, \tag{2.30}$$

Examining Eq. (2.30), we see that both the numerator and denominator in the second line are greater than or equal to those in the first line. Hence, it is not necessary that $(\alpha_{32} h_{c32})$ must be less than or equal to $(\alpha_{21} h_{c21})$, i.e., Inequality (2.23) does not have to hold The unjustified constraint on capillary pressures is therefore alleviated.

2.3.2.2 The Relations of Relative Permeability and Saturation

Based on Mualem's model 1976), the relative permeability as a function of the degree of saturation in this model is derived by modifying van Genuchten's model of two-phase flow (van Genuchten 1980):

$$k_{r1} = \bar{S}_1^{1/2} \left\{ \bar{S}_t \left[1 - \left(1 - \bar{S}_1^{1/m} \right)^m \right] \right\}^2, \tag{2.31}$$

$$k_{r2} = \left(\bar{S}_t - \bar{S}_1 \right)^{1/2} \left[\left(1 - \bar{S}_1^{1/m} \right)^m - \left(1 - \bar{S}_t^{1/m} \right)^m \right]^2, \tag{2.32}$$

$$k_{r3} = \left(1 - \bar{S}_t \right)^{1/2} \left(1 - \bar{S}_t^{1/m} \right)^{2m}. \tag{2.33}$$

Equations (2.32) and (2.33) are identical to Eqs (2.25) and (2.26) in formality, though they are derived from different relations of saturations and capillary pressures.

2.4 Numerical Results and Discussion

Four numerical examples are presented to show the feasibility and advantage of the present model. In Example 1, the initial and boundary pressure distributions satisfy the constraint ($\alpha_{21}h_{C21} \geq \alpha_{32}h_{C32}$), and thus these two constitutive models (Parker et al. 1987a; Tsai and Yeh 2012) are both executable. In the remaining examples (Examples 2, 3, and 4), however, the initial and prescribed boundary pressure distributions do not satisfy the constraint. Therefore, many available multiphase flow models which used Parker et al.'s model (e.g., Suk and Yeh 2007; Suk and Yeh 2008) either cannot yield solutions using fractional flow-approach or exclude possible solutions without physical justifications using variable-switch technique in pressure-based approach. In contrast, the present model yields simulations without excluding possible solutions, showing the advantage and capability of using the present model.

2.4.1 Example 1: Water Infiltration Problem

In this three-phase flow problem, water is infiltrated into a 40 cm long soil column shown in Fig. 2.1. The initial pressure distributions among three phases in the column satisfy the constraint, $\alpha_{21}h_{C21} > \alpha_{32}h_{C32}$. The initial conditions are the water pressure $P_1 = 7.156 \times 10^{15}\text{g/cm/day}^2$, the NAPL pressure $P_2 = 7.415 \times 10^{15}\text{g/cm/day}^2$, and the air pressure $P_3 = 7.465 \times 10^{15}\text{g/cm/day}^2$. Water infiltrates into the top of column with a constant mass flux of 10 $\text{g/cm}^2\text{/day}$ and zero NAPL and air mass fluxes. At the bottom of the column, the pressure distributions of three phases are in equilibrium with the initial state. The boundary conditions are thus specified as follows. At the top, the mass fluxes of water, NAPL, and air are $\mathbf{n} \cdot \mathbf{M}_1 = -10\text{g/cm}^2\text{/day}$, $\mathbf{n} \cdot \mathbf{M}_2 = 0$, and $\mathbf{n} \cdot \mathbf{M}_3 = 0$, respectively. At the bottom, the pressure of water is $P_1 = 7.156 \times 10^{15}\text{g/cm/day}^2$, the pressure of NAPL is $P_2 = 7.415 \times 10^{15}\text{g/cm/day}^2$, and the pressure of air is $P_3 = 7.465 \times 10^{15}\text{g/cm/day}^2$. The fluid and material properties are given in Fig. 2.1 as well. The initial time-step size is 5.0×10^{-5}day, and each subsequent time-step size is increased by 10% until a maximum time-step size of 1.0×10^{-3}day is reached.

The product of the capillary pressure and the scaling factor between NAPL and water and that between air and NAPL satisfy the constraint ($\alpha_{21}h_{C21} \geq \alpha_{32}h_{C32}$). Therefore, both the employments of Tsai and Yeh's model and Parker et al.'s model

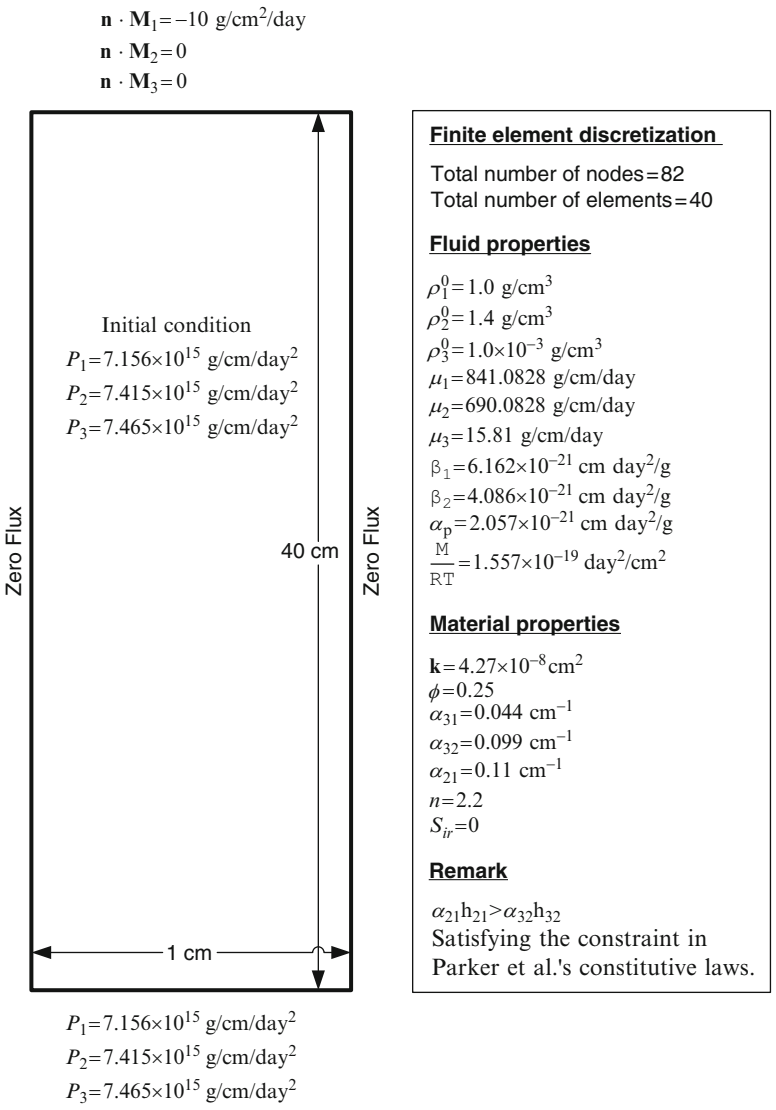

Fig. 2.1 The problem description and relevant parameters of Example 1

yield solutions. Figure 2.2 shows the solutions for saturations of water, NAPL, and air, as simulated with the present model and Parker et al.'s model. Since the expressions of saturation–capillary pressure relations in the present model and those in Parker et al.'s model are different, it is seen that the degrees of saturation for all three phases are similar in trend but quite different in magnitudes. The present

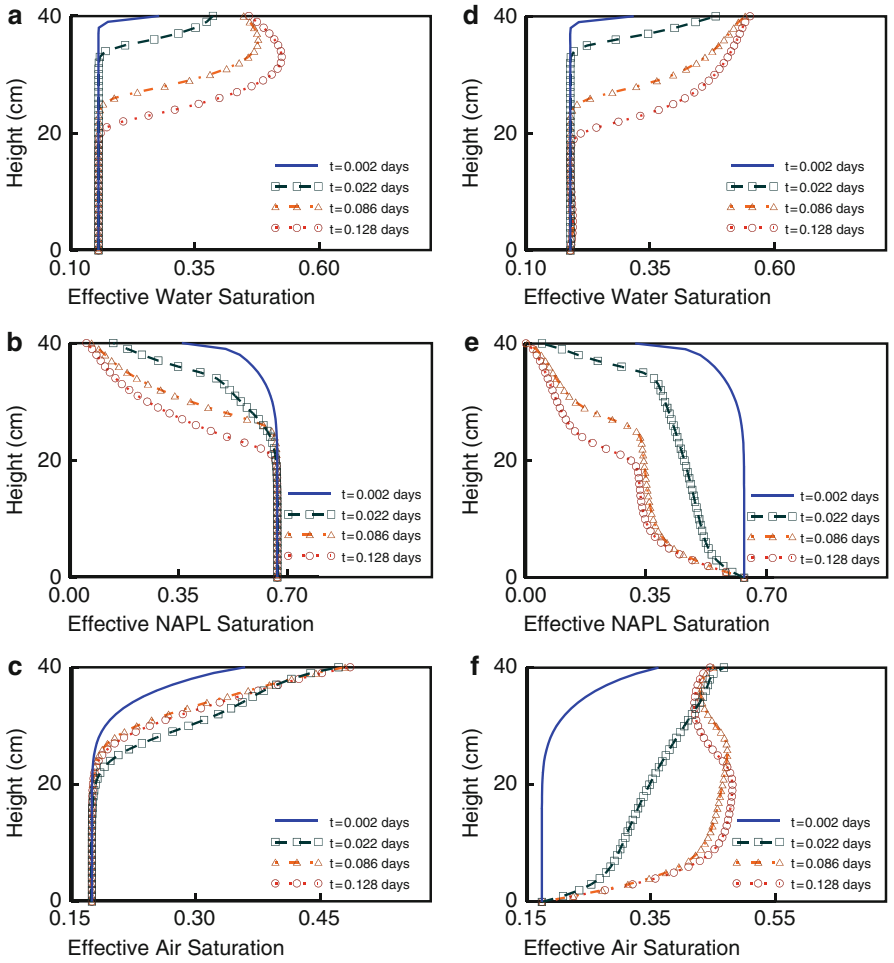

Fig. 2.2 Distributions of the degrees of saturation for Example 1: (**a**) water saturation (Tsai and Yeh's model), (**b**) NAPL saturation (Tsai and Yeh's model), (**c**) air saturation (Tsai and Yeh's model), (**d**) water saturation (Parker et al.'s model), (**e**) NAPL saturation (Parker et al.'s model), and (**f**) air saturation (Parker et al.'s model)

model yields more smoothly evolutional simulations than Parker et al.'s model. As to which model yields more reasonable results, only extensive calibrations and validations can resolve the question, which is beyond the scope of, and certainly is not the objective of, this investigation. In addition, Fig. 2.3 shows the distributions of density of air. The variation of air density providing a demonstration that compressibility is considered in the present simulator.

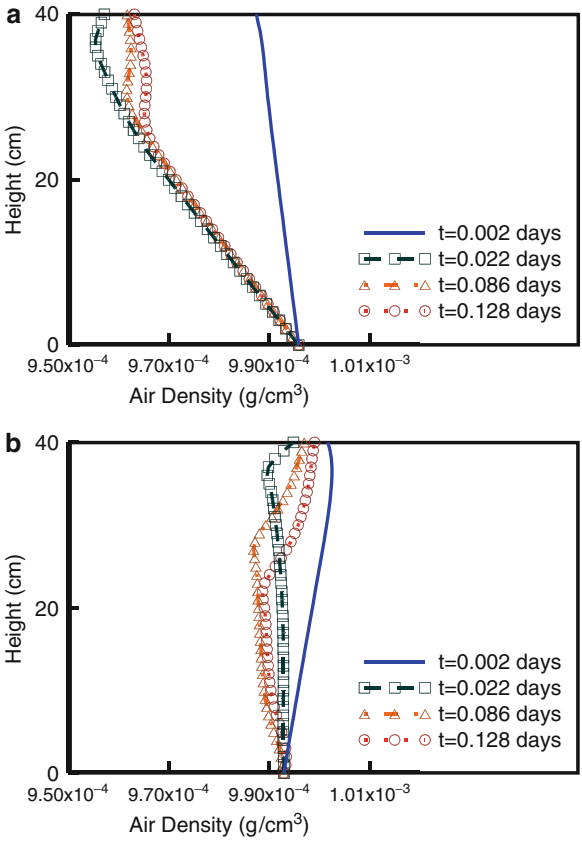

Fig. 2.3 Distributions of the density of air for Example 1: (**a**) Tsai and Yeh's model; (**b**) Parker et al.'s model

2.4.2 Example 2: Water Infiltration Problem

This example is similar to Example 1 except for the initial and bottom boundary conditions. The main differences are the initial and boundary pressure distributions do not satisfy the constraint ($\alpha_{21}h_{C21} \geq \alpha_{32}h_{C32}$) in this example while they do in Example 1. This example is presented to demonstrate the feasibility and advantage of using the Tsai and Yeh's model over that of Parker et al.'s model for the multiple flow problems of more than two fluid phases.

In many currently available pressure-based three-phase flow models that used Parker et al.'s law, negative degrees of saturation are obtained with these prescribed initial and boundary conditions. The variable-switch algorithm implemented in those models would reject these prescribed conditions. It is obvious that the rejection is due to Parker's constitutive law used, not based on any physical grounds. Therefore, simulations with those models will exclude initial and boundary conditions that might otherwise be possible. On the other hand, in many currently available

fractional flow-based three-phase flow models, the occurrence of negative degrees of saturation would have stymied the simulation. In other words, an otherwise feasibly prescribed initial and boundary pressure distribution would not produce simulations.

In this example, were Parker's model used, negative degree of saturation for NAPL would have resulted. On the other hand, the use of present model will not result in negative degrees of saturation, and thus, the prescribed initial and boundary pressure distribution would not stymie the simulation as demonstrated in this example.

Figure 2.4 shows the domain of interest. Similar to Example 1, water infiltrates into the top of the soil column with a constant mass flux of $10\,\mathrm{g/cm^2/day}$ and zero NAPL and air mass fluxes. At the bottom of the column, the pressure distributions of three phases are maintained at their initial values. The pressure distributions are specified such that they do not satisfy the constraint $(\alpha_{21}h_{C21} > \alpha_{32}h_{C32})$. The initial and bottom boundary values are given as follows. The pressure of water is $7.156 \times 10^{15}\mathrm{g/cm/day^2}$, the pressure of NAPL is $7.235 \times 10^{15}\,\mathrm{g/cm/day^2}$, and the pressure of air is $7.465 \times 10^{15}\mathrm{g/cm/day^2}$. The boundary conditions at the top are the same as that in Example 1: the mass fluxes of water, NAPL, and air are $\mathbf{n} \cdot \mathbf{M}_1 = -10\mathrm{g/cm^2/day}$, $\mathbf{n} \cdot \mathbf{M}_2 = 0$, and $\mathbf{n} \cdot \mathbf{M}_3 = 0$, respectively. The fluid and material properties are given in Fig. 2.4. The initial time-step size is 5.0×10^{-5}day, and each subsequent time-step size is increased by 10% until a maximum time-step size of 1.0×10^{-3}day is reached.

Plausible solutions are obtained with the present model. The solution for degrees of saturation in each phase is depicted in Fig. 2.5. It is seen that NAPL and air are displaced downward from the top of the soil column, while water infiltrates into the column, as expected. Additionally, because NAPL is squeezed by the constant infiltration of water, it is observed that the peak of NAPL saturation moves downward with increasing simulation times, as expected. The variations in air density are shown in Fig. 2.6. It is seen that the air density increases while water constantly infiltrates into the system, as expected.

The initial and prescribed boundary pressure distributions in Example 2 do not satisfy the constraint inherent in Parker et al.'s model. Therefore, for such pressure distributions, using Parker et al.'s model either will not yield solutions using fractional flow-based models or may generate wrong solutions using pressure-based models due to the switch of primary variables. In contrast, with the use of Tsai and Yeh's model, the present multiphase flow model is more physically realistic and is capable of simulating the problems which cover all possible pressure distributions.

2.4.3 Example 3: NAPL Infiltration Problem

In Example 3, NAPL constantly infiltrates into a 165 cm long by 65 cm high soil block shown in Fig. 2.7. The initial conditions of three phases are the following: the water saturation is $S_1 = 0.1$, the NAPL saturation is $S_2 = 0.1$, and the air saturation is $S_3 = 0.8$. Since a $10\,\mathrm{g/cm^2/day}$ NAPL mass flux, zero water, and air

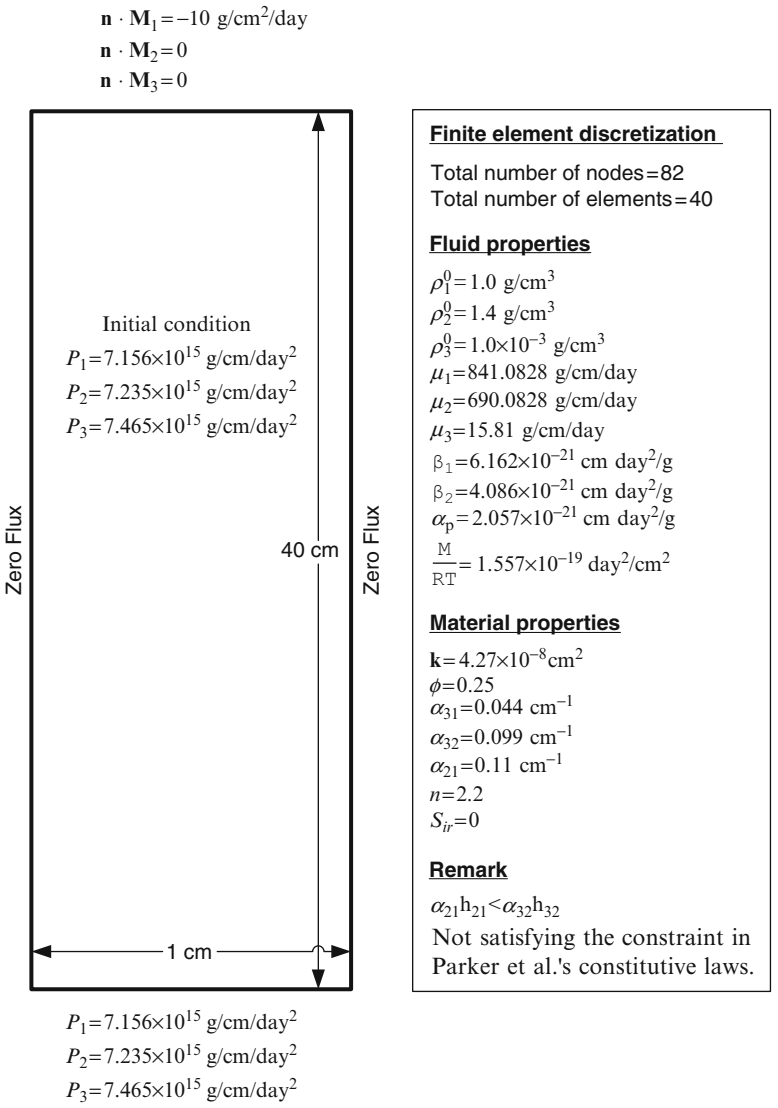

Fig. 2.4 The problem description and relevant parameters of Example 2

mass fluxes infiltrate into an opening on the top, the boundary conditions therein are specified as the mass flux of water is $\mathbf{n} \cdot \mathbf{M}_1 = 0$, the mass flux of NAPL is $\mathbf{n} \cdot \mathbf{M}_2 = -10\mathrm{g/cm^2/day}$, and the mass flux of air is $\mathbf{n} \cdot \mathbf{M}_3 = 0$. On the left side of the block, the pressure distributions are specified as follows: the pressure of water is $P_1 = 7.234 \times 10^{15}\,\mathrm{g/cm/day^2}$, the pressure of NAPL is $P_2 = 7.336 \times 10^{15}\,\mathrm{g/cm/day^2}$, and the pressure of air is $P_3 = 7.611 \times 10^{15}\,\mathrm{g/cm/day^2}$. On the right side, the

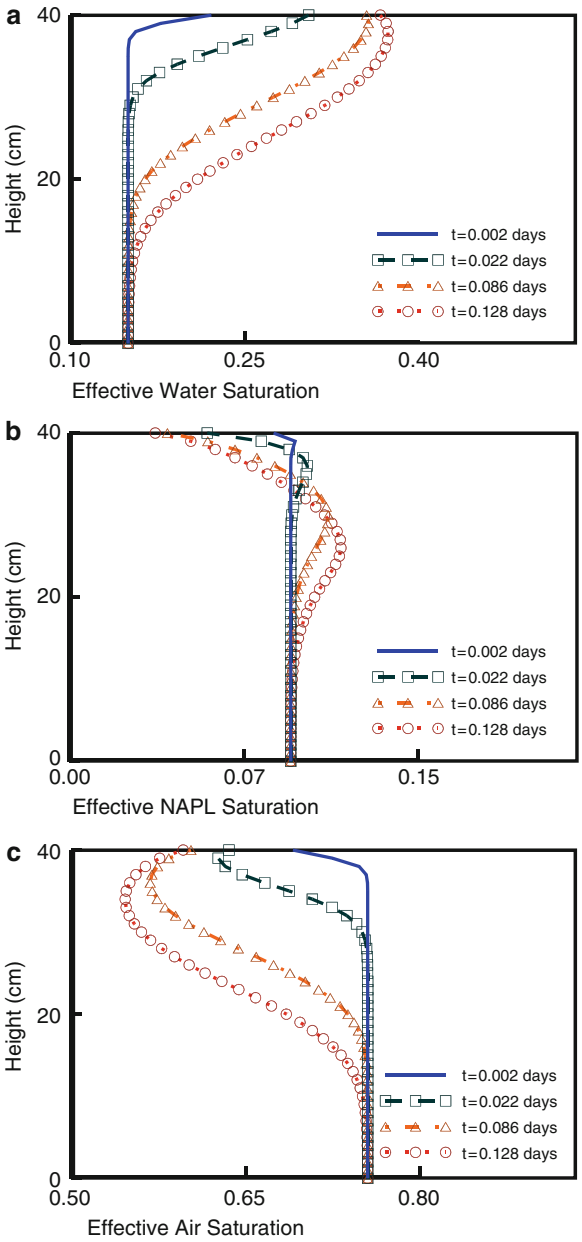

Fig. 2.5 Distributions of the degrees of saturation for Example 2: (**a**) water saturation, (**b**) NAPL saturation, and (**c**) air saturation

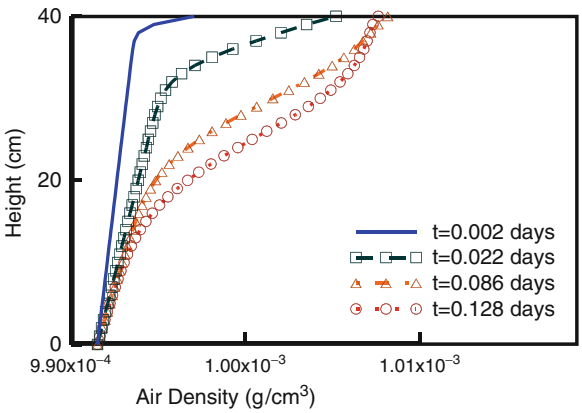

Fig. 2.6 Distributions of the density of air for Example 2

pressure distribution is the pressure of water is $P_1 = 7.087 \times 10^{15}\,\mathrm{g/cm/day^2}$, the pressure of NAPL is $P_2 = 7.189 \times 10^{15}\,\mathrm{g/cm/day^2}$, and the pressure of air is $P_3 = 7.465 \times 10^{15}\,\mathrm{g/cm/day^2}$. On the bottom, the boundary condition is specified as the water saturation is $S_1 = 0.1$, the NAPL saturation is $S_2 = 0.1$, and the air saturation is $S_3 = 0.8$. The block is pumped with a flux rate $-50\,\mathrm{cm^3/day}$ at five well points 0.2 days after the infiltration began. The fluid and material properties are given in Fig. 2.7 as well. The initial time-step size is 1.0×10^{-4}day, and each subsequent time-step size is increased by 10% until a maximum time-step size of 1.0×10^{-3}day is reached.

The distributions of NAPL, water, and air saturation through time are given in Figs. 2.8, 2.9, and 2.10, respectively. It is seen that the water and NAPL saturations approximate to zero around the well due to the effect of pumping. In Fig. 2.8, the pumping affects the distributions of NAPL contour obviously at 0.284 and 0.984 days but has little effects at 2.984 days. The continuous pumping leads the NAPL saturation near well points to approximate zero and hence reduces its conductivity. Therefore the infiltrated NAPL will not flow to the well. As a result, the pore space near the well is occupied mostly by the air phase (Fig. 2.10) via its high conductivity. Figure 2.9 indicates that the water saturation changes little through the entire domain of interest except for a small region near the well. This example implies that a pump and treat strategy of NAPL removal would not work for this particular case.

2.4.4 Example 4: NAPL Infiltration Problem

In this example, NAPL infiltrates into a 165 cm long by 65 cm highly unsaturated block with zero mass fluxes of water and air shown in Fig. 2.11. The majority of the block is filled with sands. Three additional materials are included in small portions of the domain, which are clay, silt, and gravel. The initial conditions of three phases

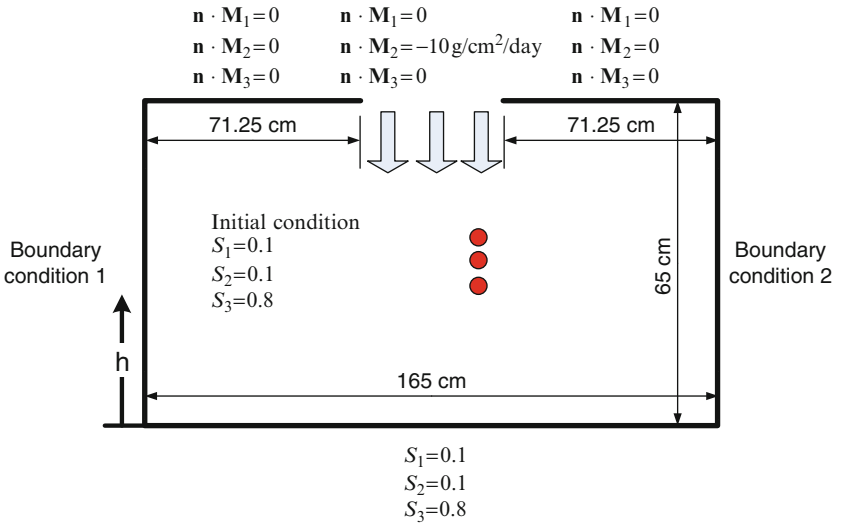

Boundary condition 1

$P_1=7.23355\times10^{15}\text{-}\rho_1^0$ gh g/cm/day^2

$P_2=7.33557\times10^{15}\text{-}\rho_1^0$ gh g/cm/day^2

$P_3=7.61132\times10^{15}\text{-}\rho_1^0$ gh g/cm/day^2

Boundary condition 2

$P_1=7.08723\times10^{15}\text{-}\rho_1^0$ gh g/cm/day^2

$P_2=7.18925\times10^{15}\text{-}\rho_1^0$ gh g/cm/day^2

$P_3=7.46450\times10^{15}\text{-}\rho_1^0$ gh g/cm/day^2

Finite element discretization

Total number of nodes = 1485
Total number of elements = 1408

Material properties

$\mathbf{k}=4.27\times10^{-8}$ cm^2
$\phi=0.25$
$\alpha_{31}=0.044$ cm^{-1}
$\alpha_{32}=0.099$ cm^{-1}
$\alpha_{21}=0.11$ cm^{-1}
$n=2.2$
$S_{ir}=0$

Fluid properties

$\rho_1^0=1.0$ g/cm^3
$\rho_2^0=1.4$ g/cm^3
$\rho_3^0=1.0\times10^{-3}$ g/cm^3
$\mu_1=841.0828$ g/cm/day
$\mu_2=690.0828$ g/cm/day
$\mu_3=15.81$ g/cm/day
$\beta_1=6.162\times10^{-21}$ cm day^2/g
$\beta_2=4.086\times10^{-21}$ cm day^2/g
$\alpha_s=2.057\times10^{-21}$ cm day^2/g
$\frac{M}{RT}=1.557\times10^{-19}$ day^2/cm^2

Pumping well

Well position

(97.5, −28.4375)
(97.5, −26.40625)
(97.5, −24.375)
(97.5, −22.34375)
(97.5, −20.3125)

Pumping rate

0	if time < 0.2 days
−50 cm^3/day	if time < 0.2 days

Fig. 2.7 The problem description and relevant parameters of Example 3

are: the water saturation is $S_1 = 0.2$, the NAPL saturation is $S_2 = 0.1$, and the air saturation is $S_3 = 0.7$. Since a $10\,\mathrm{g/cm^2/day}$ NAPL mass flux, zero water, and air mass fluxes infiltrate into an opening on the top, the boundary conditions therein are specified as: the mass flux of water is $\mathbf{n}\cdot\mathbf{M}_1 = 0$, the mass flux of NAPL is $\mathbf{n}\cdot\mathbf{M}_2 = -10\mathrm{g/cm^2/day}$, and the mass flux of air is $\mathbf{n}\cdot\mathbf{M}_3 = 0$. On the left and right sides, the pressure distributions of three phases are specified as follows: the

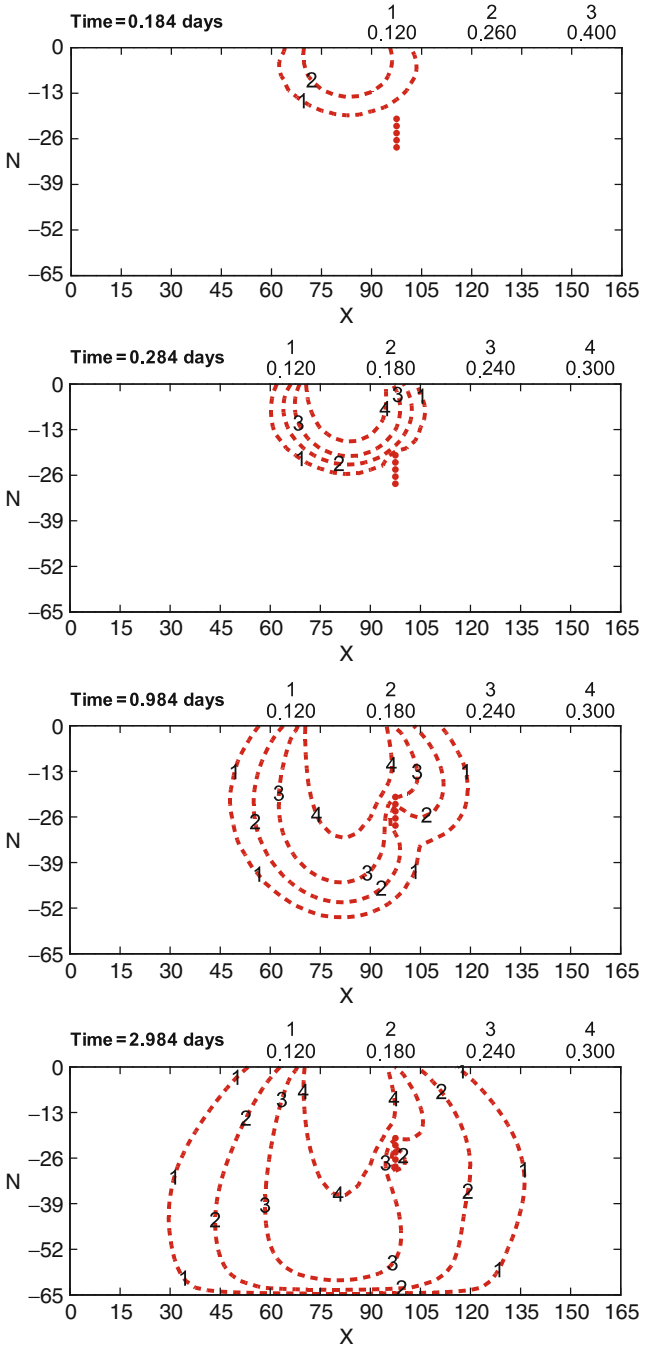

Fig. 2.8 Distributions of the degrees of saturation of NAPL for Example 3

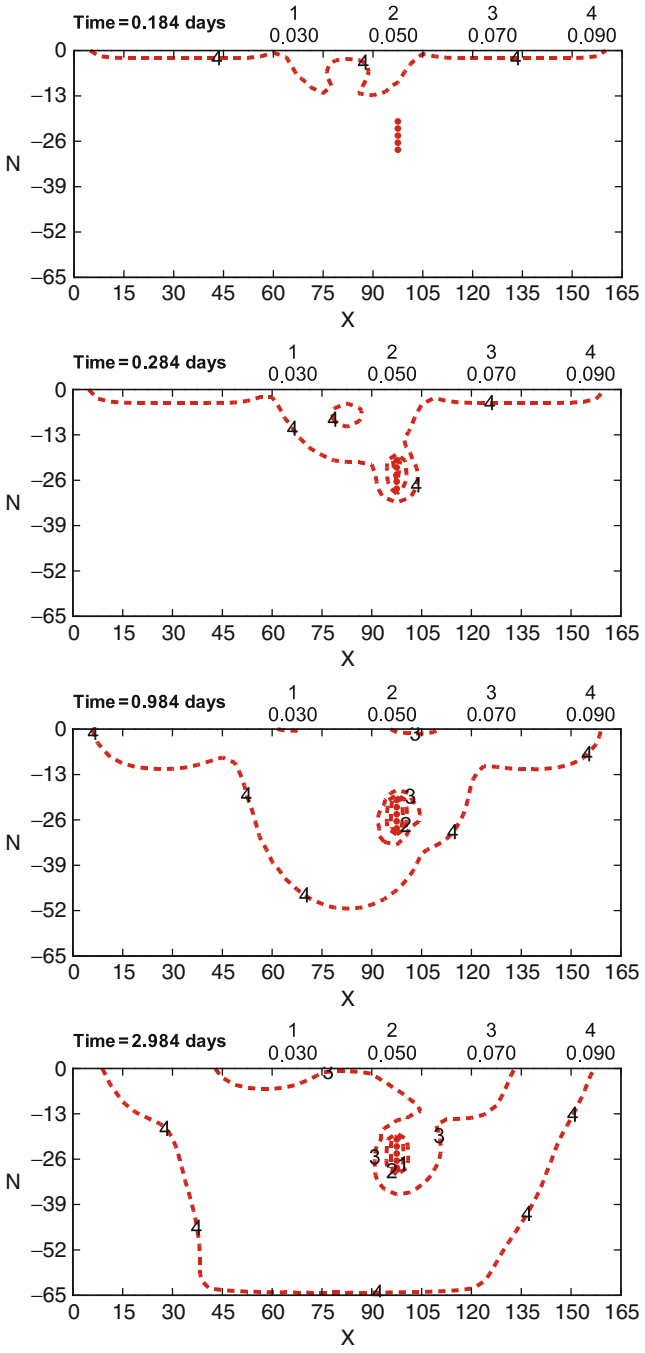

Fig. 2.9 Distributions of the degrees of saturation of water for Example 3

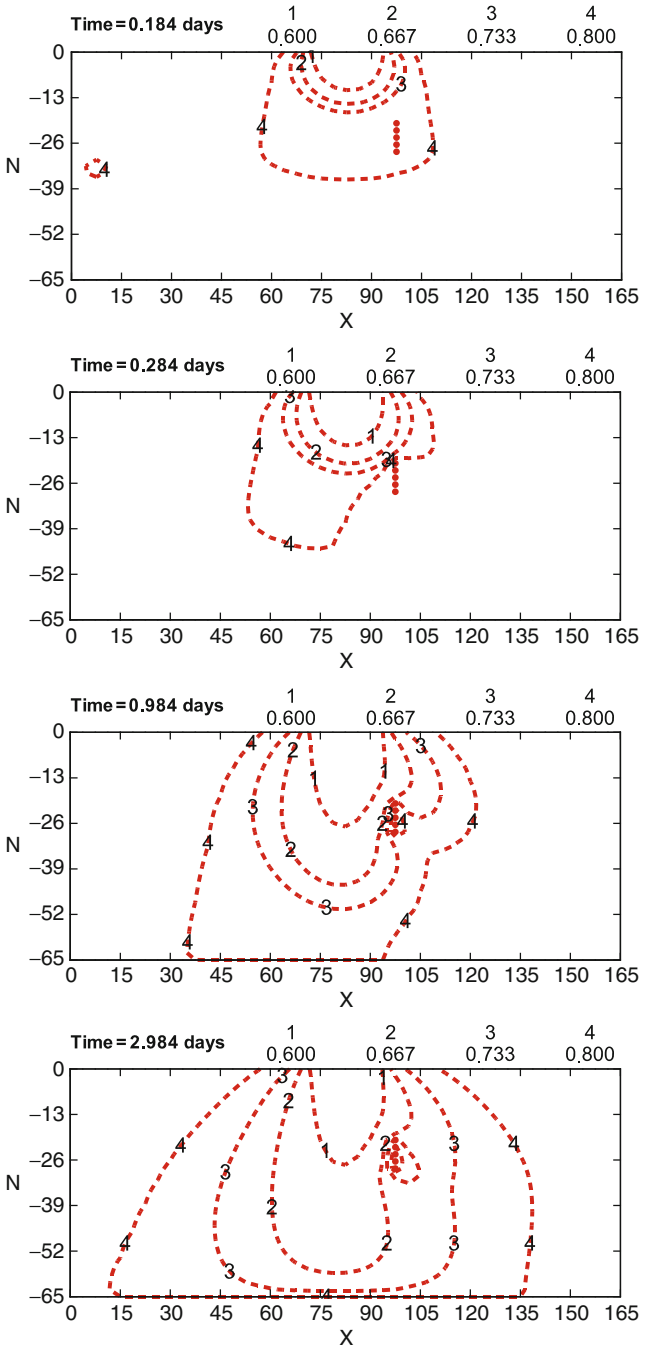

Fig. 2.10 Distributions of the degrees of saturation of air for Example 3

pressure of water is $P_1 = 7.351 \times 10^{15}\,\mathrm{g/cm/day^2}$, the pressure of NAPL is $P_2 = 7.420 \times 10^{15}\,\mathrm{g/cm/day^2}$, and the pressure of air is $P_3 = 7.611 \times 10^{15}\,\mathrm{g/cm/day^2}$. On the bottom, the boundary condition is specified as: the water saturation is $S_1 = 0.2$, the NAPL saturation is $S_2 = 0.1$, and the air saturation is $S_3 = 0.7$. The fluid properties are also given in Fig. 2.11. The initial time-step size is 1.0×10^{-4}day, and each subsequent time-step size is increased by 10% until a maximum time-step size of 1.0×10^{-3}day is reached.

The distributions of degrees of saturation for NAPL, water, and air are depicted in Figs.2.12, 2.13, and 2.14, respectively. Two liquid phases (water and NAPL) behave similarly in this highly heterogeneous system of media. When they reach the gravel, they flow through it quickly because the permeability of gravel is much higher than that of the sand. When they reach the silt, they flow on its surface and move sideway and flow down with a small portion going through the silt. When they reach the very impermeable clay, they almost completely float on its surface and flow sideway then downward, with very little going through the clay. It is seen from Fig. 2.14 that as NAPL infiltrates, air is to first move to both sides and then upward because of its low density. As the air moves up, it bypasses the relatively impermeable silt and clay but goes through the very permeable gravel quickly. The results show the capability of the present model to generate reasonable simulations for the NAPL infiltration problem.

2.5 Conclusions

In this investigation, the constitutive law proposed by Tsai and Yeh is successfully implemented in a fractional flow-based multiphase flow model to simulate compressible subsurface flow problems with different possible pressure distributions. To demonstrate the feasibility and advantage of the developed model, four examples are presented. The results clearly show the feasibility and advantage of implementing the new constitutive law to simulate compressible flow problems, especially with the cases that prescribed pressure distributions do not satisfy the constraint required by Parker et al.'s model. With the implementation of the new saturationcapillary pressure relationship, plausible solutions are obtained with all possible initial and boundary pressure distributions. In summary, the implementation of the advanced constitutive law makes the present multiphase flow model complete and physically realistic to simulate the compressible flow problems with all possible pressure distributions.

Acknowledgements Research is supported by National Science Council under Contract No. NSC 99–2116-M-008–020 with National Central University.

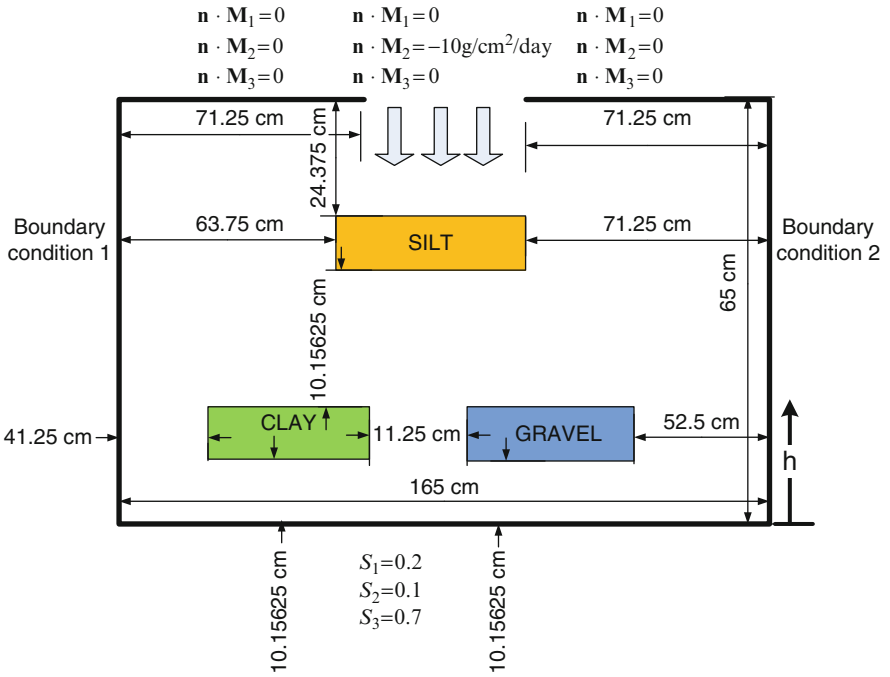

Initial condition	Boundary condition 1	Boundary condition 2
S_1= 0.2	P_1=7.35063×10^{15}-ρ_1^0 gh g/cm/day^2	P_1=7.35063×10^{15}-ρ_1^0 gh g/cm/day^2
S_2=0.1	P_2=7.42017×10^{15}-ρ_1^0 gh g/cm/day^2	P_2=7.42017×10^{15}-ρ_1^0 gh g/cm/day^2
S_3=0.7	P_3=7.61132×10^{15}-ρ_1^0 gh g/cm/day^2	P_3=7.61132×10^{15}-ρ_1^0 gh g/cm/day^2

Finite element discretization

Total number of nodes = 1485
Total number of elements = 1408

Material properties

$\mathbf{k}$=4.27×10^{-8} cm^2
ϕ=0.25
α_{31}=0.044 cm^{-1}
α_{32}=0.099 cm^{-1}
α_{21}=0.11 cm^{-1}
n=2.2
S_{ir}=0

GRAVEL
$\mathbf{k}$=4.27×10^{-6} cm^2
ϕ=0.25

CLAY
$\mathbf{k}$=4.27×10^{-12} cm^2
ϕ=0.40

SILT
$\mathbf{k}$=4.27×10^{-10} cm^2
ϕ=0.35

Fluid properties

ρ_1^0=1.0 g/cm^3
ρ_2^0=1.4 g/cm^3
ρ_3^0=1.0×10^{-3} g/cm^3
μ_1=841.0828 g/cm/day
μ_2=690.0828 g/cm/day
μ_3=15.81 g/cm/day
β_1=6.162×10^{-21} cm day^2/g
β_2=4.086×10^{-21} cm day^2/g
α_s=2.057×10^{-21} cm day^2/g
$\frac{M}{RT}$=1.557×10^{-19} day^2/cm^2

Fig. 2.11 The problem description and relevant parameters of Example 4

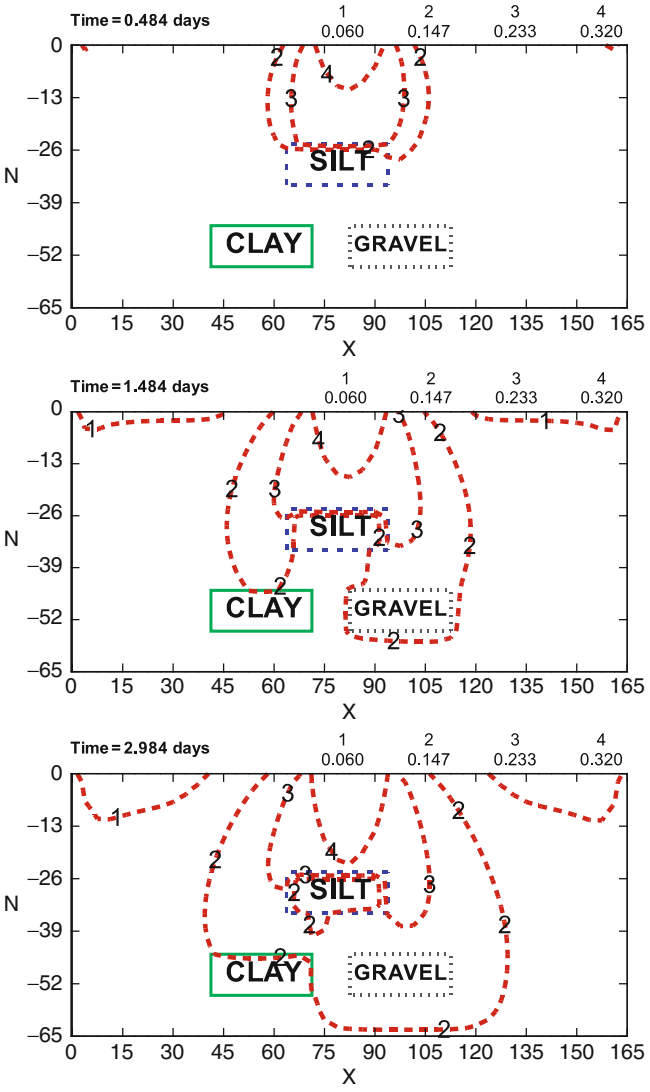

Fig. 2.12 Distributions of the degrees of saturation of NAPL for Example 4

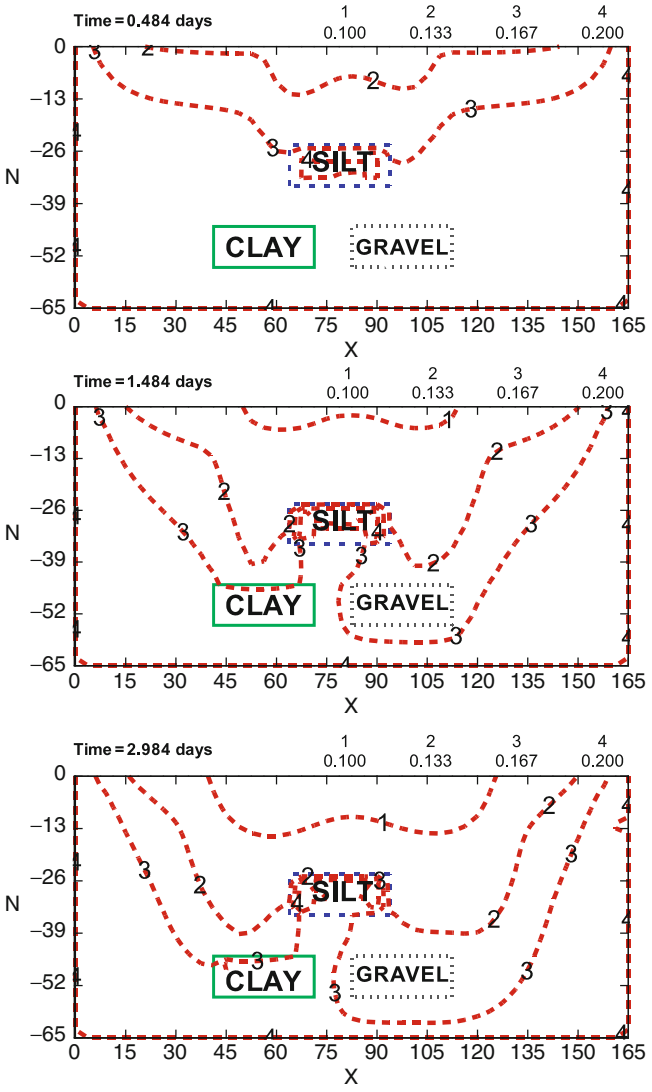

Fig. 2.13 Distributions of the degrees of saturation of water for Example 4

Appendix A: Numerical Discretizations with FEM

The governing equation for the total pressure, Eq. (2.5), is discretized with the standard Galerkin FEM as follows:

$$[C^p]\left\{\frac{\partial P_t}{\partial t}\right\}+[C^p_{s1}]\left\{\frac{\partial S_1}{\partial t}\right\}+[C^p_{st}]\left\{\frac{\partial S_t}{\partial t}\right\}+[DD_p]\{P_t\}=\{f_p\}, \qquad \text{(A.1)}$$

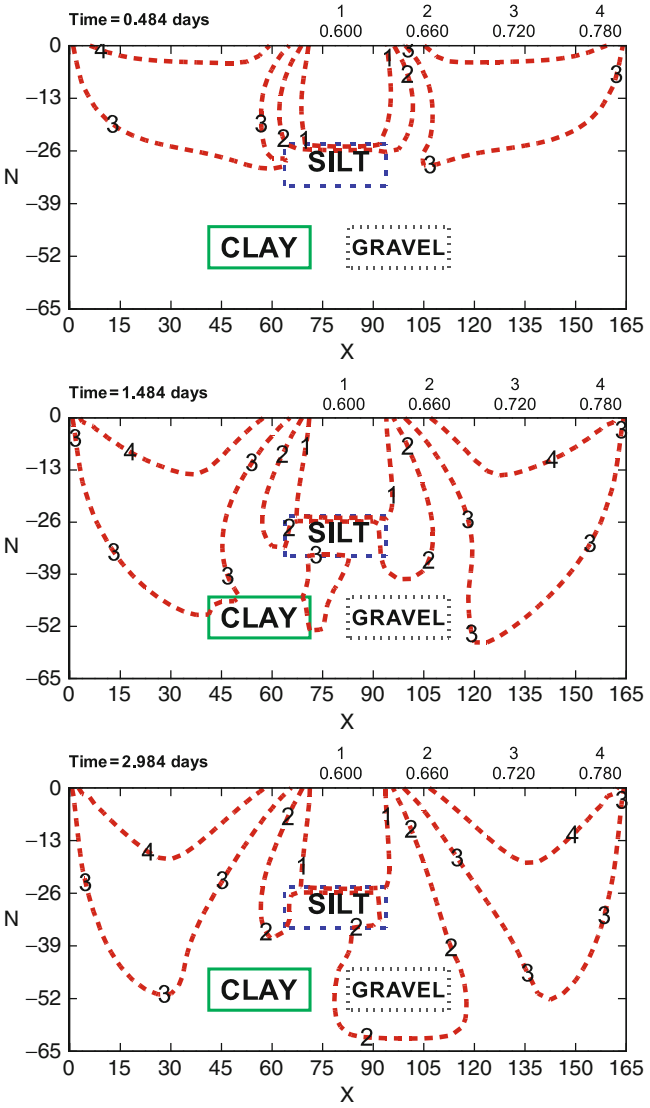

Fig. 2.14 Distributions of the degrees of saturation of air for Example 4

in which

$$[C^p]_{i,j} = \int_{\Omega} (C_{pt}) \nabla N_i \cdot \nabla N_j \mathrm{d}R, \tag{A.2}$$

$$\left[C_{s1}^{p}\right]_{i,j} = \int_{\Omega} (C_{s1}) \nabla N_i \cdot \nabla N_j \mathrm{d}R, \tag{A.3}$$

$$\left[C_{st}^{p}\right]_{i,j} = \int_{\Omega} (C_{st}) \nabla N_i \cdot \nabla N_j \mathrm{d}R, \tag{A.4}$$

$$\left[DD_p\right]_{i,j} = \int_{\Omega} \nabla N_i \cdot \nabla N_j \mathrm{d}R, \tag{A.5}$$

$$\left\{f_p\right\}_i = -\int_{\Omega} \nabla N_i \bullet \left[\overline{\rho} g \nabla z\right] \mathrm{d}R - \int_{B} \mathbf{n} \bullet \left[N_i \left(\mathbf{M}_t\right)\right] \mathrm{d}B + \int_{\Omega} N_i \left[Q_t\right] \mathrm{d}R, \tag{A.6}$$

where $[C^p]$ is the mass matrix associated with total pressure, $[C_{s1}^p]$ is the mass matrix associated with water saturation for total pressure, $[C_{st}^p]$ is the mass matrix associated with total liquid saturation for total pressure, $[DD_p]$ is the dispersion-diffusion matrix associated with P_t in the governing equation for total pressure, and $\{f_p\}$ is the flux due to advection, dispersion-diffusion, and gravity in the governing equation for total pressure.

The governing equations for the saturations of water and total liquid, Eqs. (2.15) and (2.16), are discretized by the standard Galerkin and the upstream FEMs. The optimized weighting parameters for the upstream FEM are found in the literature (e.g., Carrano and yeh 1995; Christie et al. 1976). Other more robust numerical discretization methods may be employed, but that will not alter the key points addressed in this chapter. The formulations are given as follows:

$$\begin{aligned}&\left[C_1^p\right]\left\{\frac{\partial P_t}{\partial t}\right\} + \left[C_1^w\right]\left\{\frac{\partial S_1}{\partial t}\right\} + \left[C_1^t\right]\left\{\frac{\partial S_t}{\partial t}\right\} + \left[ADW_1\right]\left\{S_1\right\} + \left[ADT_1\right]\left\{S_t\right\} + \left[DDW_1\right]\left\{S_1\right\} \\ &\quad + \left[DDT_1\right]\left\{S_t\right\} + \left[DST_1\right]\left\{S_1\right\} = \left\{f_1\right\},\end{aligned} \tag{A.7}$$

and

$$\begin{aligned}&\left[C_2^p\right]\left\{\frac{\partial P_t}{\partial t}\right\} + \left[C_2^w\right]\left\{\frac{\partial S_1}{\partial t}\right\} + \left[C_2^t\right]\left\{\frac{\partial S_t}{\partial t}\right\} + \left[ADW_2\right]\left\{S_1\right\} + \left[ADT_2\right]\left\{S_t\right\} + \left[DDW_2\right]\left\{S_1\right\} \\ &\quad + \left[DDT_2\right]\left\{S_t\right\} + \left[DST_2\right]\left\{S_t\right\} = \left\{f_2\right\},\end{aligned} \tag{A.8}$$

in which

$$\left[C_1^p\right]_{i,j} = \int_{\Omega} \left(\phi S_1 \frac{\partial \rho_1}{\partial P_1} - \kappa_1 C_{pt} + \rho_1 S_1 \alpha_p\right) N_i N_j dR, \tag{A.9}$$

$$\left[C_1^w\right]_{i,j} = \int_{\Omega} \left(\phi S_1 \frac{\partial \rho_1}{\partial P_1} (1-\kappa_1) \frac{\mathrm{d}P_{C12}}{\mathrm{d}S_1} + \rho_1 \phi - \kappa_1 C_{s1} + \rho_1 S_1 \alpha_p \left[P_{C12} + (S_1 - \kappa_1) \frac{\mathrm{d}P_{C12}}{\mathrm{d}S_1}\right]\right) N_i N_j \mathrm{d}R, \tag{A.10}$$

$$\left[C_1^t\right]_{i,j} = \int_{\Omega} \left(\phi S_1 \frac{\partial \rho_1}{\partial P_1} \kappa_3 \frac{\mathrm{d}P_{C23}}{\mathrm{d}S_t} - \kappa_1 C_{st} + \rho_1 S_1 \alpha_p \left[P_{C23} + (S_t - 1 + \kappa_3) \frac{\mathrm{d}P_{C23}}{\mathrm{d}S_t}\right]\right) N_i N_j \mathrm{d}R, \tag{A.11}$$

$$[ADW_1]_{i,j} = \int_{\Omega} W_i \frac{\mathrm{d}\kappa_1}{\mathrm{d}S_1}\mathbf{M}_t \bullet \nabla N_j \mathrm{d}R - \int_{\Omega} W_i \left[\frac{\mathrm{d}\left(\kappa_1 \boldsymbol{\kappa} \bullet (\rho_1 - \overline{\rho})\, g\nabla z\right)}{\mathrm{d}S_1}\right] \bullet \nabla N_j \mathrm{d}R, \tag{A.12}$$

$$[ADT_1]_{i,j} = \int_{\Omega} W_i \frac{\mathrm{d}\kappa_1}{\mathrm{d}S_t}\mathbf{M}_t \bullet \nabla N_j \mathrm{d}R - \int_{\Omega} W_i \left[\frac{\mathrm{d}\left(\kappa_1 \boldsymbol{\kappa} \bullet (\rho_1 - \overline{\rho})\, \rho_1 g\nabla z\right)}{\mathrm{d}S_t}\right] \bullet \nabla N_j \mathrm{d}R, \tag{A.13}$$

$$[DDW_1]_{i,j} = \int_{\Omega} \nabla N_i \bullet \left[\kappa_1 \boldsymbol{\kappa} \bullet (1-\kappa_1)\frac{\mathrm{d}P_{C12}}{\mathrm{d}S_1}\nabla N_j\right]\mathrm{d}R + \int_{\Omega} \nabla N_i \bullet \left[\kappa_1 \boldsymbol{\kappa} \bullet \kappa_3 \frac{\mathrm{d}P_{C23}}{\mathrm{d}S_1}\nabla N_j\right]\mathrm{d}R, \tag{A.14}$$

$$[DDT_1]_{i,j} = \int_{\Omega} \nabla N_i \bullet \left[\kappa_1 \boldsymbol{\kappa} \bullet (1-\kappa_1)\frac{\mathrm{d}P_{C12}}{\mathrm{d}S_t}\nabla N_j\right]\mathrm{d}R + \int_{\Omega} \nabla N_i \bullet \left[\kappa_1 \kappa \bullet \kappa_3 \frac{\mathrm{d}P_{C23}}{\mathrm{d}S_t}\nabla N_j\right]\mathrm{d}R, \tag{A.15}$$

$$[DST_1]_{i,j} = \int_{\Omega} N_i \left(\frac{\kappa_1 Q_t - Q_1}{S_1}\right) N_i \mathrm{d}R, \tag{A.16}$$

$$\{f_1\}_i = \int_B N_i \mathbf{n} \bullet [\kappa_1 \mathbf{M}_t]\mathrm{d}B - \int_B N_i \mathbf{n} \bullet [\mathbf{M}_1]\mathrm{d}B - \int_B N_i \mathbf{n} \bullet [\kappa_1 \kappa \bullet (\rho_1 - \overline{\rho})\, g\nabla z]\mathrm{d}B, \tag{A.17}$$

$$\left[C_2^p\right]_{i,j} = -\int_{\Omega} \left(\phi S_3 \frac{\partial \rho_3}{\partial P_3} - \kappa_3 C_{pt} + \rho_3 S_3 \alpha_p\right) N_i N_j \mathrm{d}R, \tag{A.18}$$

$$[C_2^w]_{i,j} = \int_{\Omega} \left(\phi S_3 \frac{\partial \rho_3}{\partial P_3}\kappa_1 \frac{\mathrm{d}P_{C12}}{\mathrm{d}S_1} + \kappa_3 C_{s1} - \rho_3 S_3 \alpha_p \left[P_{C12} + (S_1 - \kappa_1)\frac{\mathrm{d}P_{C12}}{\mathrm{d}S_1}\right]\right) N_i N_j \mathrm{d}R, \tag{A.19}$$

$$\left[C_2^t\right]_{i,j} = \int_{\Omega} \left(\phi S_3 \frac{\partial \rho_3}{\partial P_3}(1-\kappa_3)\frac{\mathrm{d}P_{C23}}{\mathrm{d}S_t} + \kappa_3 C_{st} + \rho_3 \phi - \rho_3 S_3 \alpha_p \left[P_{C23} + (S_t - 1 + \kappa_3)\frac{\mathrm{d}P_{C23}}{\mathrm{d}S_t}\right]\right) N_i N_j \mathrm{d}R, \tag{A.20}$$

$$[ADW_2]_{i,j} = -\int_{\Omega} W_i \mathbf{M}_t \bullet \left[\frac{\mathrm{d}\kappa_3}{\mathrm{d}S_1}\nabla N_j\right]\mathrm{d}R + \int_{\Omega} W_i \left[\frac{\mathrm{d}\left(\kappa_3 \boldsymbol{\kappa} \bullet (\rho_3 - \overline{\rho})\, g\nabla z\right)}{\mathrm{d}S_1}\right] \cdot \nabla N_j \mathrm{d}R, \tag{A.21}$$

$$[ADT_2]_{i,j} = -\int_{\Omega} W_i \mathbf{M}_t \bullet \left[\frac{\mathrm{d}\kappa_3}{\mathrm{d}S_t}\nabla N_j\right]\mathrm{d}R + \int_{\Omega} W_i \left[\frac{\mathrm{d}\left(\kappa_3 \boldsymbol{\kappa} \bullet (\rho_3 - \overline{\rho})\, g\nabla z\right)}{\mathrm{d}S_t}\right] \bullet \nabla N_j \mathrm{d}R, \tag{A.22}$$

$$[DDW_2]_{i,j} = \int_{\Omega} \nabla N_i \bullet \left[\kappa_3 \boldsymbol{\kappa} \bullet \kappa_1 \frac{\mathrm{d}P_{C12}}{\mathrm{d}S_1}\nabla N_j\right]\mathrm{d}R + \int_{\Omega} \nabla N_i \bullet \left[\kappa_3 \boldsymbol{\kappa} \bullet (1-\kappa_3)\frac{\mathrm{d}P_{C23}}{\mathrm{d}S_1}\nabla N_j\right]\mathrm{d}R, \tag{A.23}$$

$$[DDT_2]_{i,j} = \int_{\Omega} \nabla N_i \bullet \left[\kappa_3 \boldsymbol{\kappa} \bullet \kappa_1 \frac{\mathrm{d}P_{C12}}{\mathrm{d}S_t}\nabla N_j\right]\mathrm{d}R + \int_{\Omega} \nabla N_i \bullet \left[\kappa_3 \boldsymbol{\kappa} \bullet (1-\kappa_3)\frac{\mathrm{d}P_{C23}}{\mathrm{d}S_t}\nabla N_j\right]\mathrm{d}R, \tag{A.24}$$

$$[DST_2]_{i,j} = \int_{\Omega} N_i \left(\frac{-\kappa_3 Q_t + Q_3}{S_t}\right) N_i \mathrm{d}R, \tag{A.25}$$

$$\{f_2\}_i = -\int_B N_i \mathbf{n} \bullet [\kappa_3 \mathbf{M}_t]\mathbf{d}B + \int_B N_i \mathbf{n} \bullet [\mathbf{M}_3]\mathbf{d}B + \int_B N_i \mathbf{n} \bullet [\kappa_3 \boldsymbol{\kappa} \bullet (\rho_3 - \overline{\rho})\, g\nabla z]\mathbf{d}B, \tag{A.26}$$

where $[C_1^p]$ is the mass matrix associated with total pressure for water saturation; $[C_1^w]$ is the mass matrix associated with water saturation; $[C_1^t]$ is the mass matrix associated with total liquid saturation for water saturation; $[ADW_1]$ is the advection and gravity matrix associated with water saturation; $[ADT_1]$ is the advection and gravity matrix associated with total liquid saturation; $[DDW_1]$ is the dispersion-

diffusion matrix associated with water saturation; $[DDT_1]$ is the dispersion-diffusion matrix associated with total liquid saturation; $[DST_1]$ is the matrix from the sink or source; $\{f_1\}$ is the flux due to advection, dispersion-diffusion, and gravity; $[C_2^p]$ is the mass matrix associated with total pressure for total liquid saturation; $[C_2^s]$ is the mass matrix associated with water saturation for total liquid saturation; $[C_2^t]$ is the mass matrix associated with total liquid saturation; $[ADW_2]$ is the advection and gravity matrix associated with water saturation; $[ADT_2]$ is the advection and gravity matrix associated with total liquid saturation; $[DDW_2]$ is the dispersion-diffusion matrix associated with water saturation; $[DDT_2]$ is the dispersion-diffusion matrix associated with total liquid saturation; $[DST_2]$ is the matrix from the sink or source; $\{f_2\}$ is the flux due to advection, dispersion-diffusion, and gravity; W_i is the upstream weighting function; N_i is the Galerkin interpolation function; $\mathbf{n}$ is the outward normal vector; Ω is the region of interest; and B is the boundary. Note that the subscripts 1 and 2 in the definitions of all matrices denote the first and second equation of two saturation equations, respectively. By assembling Eqs. (A.7) and (A.8), the resulting coupled matrix for saturations of water and total liquid is given as follows:

$$\begin{bmatrix} C_1^w & C_1^t \\ C_2^w & C_2^t \end{bmatrix} \begin{Bmatrix} \frac{\partial S_1}{\partial t} \\ \frac{\partial S_t}{\partial t} \end{Bmatrix} + \begin{bmatrix} DDW_1 + ADW_1 + DST_1 & DDT_1 + ADT_1 \\ DDW_2 + ADW_2 & DDT_2 + ADT_2 + DST_2 \end{bmatrix} \begin{Bmatrix} S_1 \\ S_t \end{Bmatrix} = \begin{Bmatrix} f_1 \\ f_2 \end{Bmatrix} - \begin{Bmatrix} C_1^p \frac{\partial P_t}{\partial t} \\ C_2^p \frac{\partial P_t}{\partial t} \end{Bmatrix}. \tag{A.27}$$

To obtain the solutions for the total pressure, saturations of water, and total liquid, we use the Bi-CGSTAB method proposed by vant der Vorst (1992).

References

Binning P, Celia MA (1999) Practical implementation of the fractional flow approach to multi-phase flow simulation. Adv Water Resour 22:461–478

Carrano CS Jr, Yeh GT (1995) A Fourier analysis of dynamic optimization of the Petrov-Galerkin finite element method. Int J Numer Methods Eng 38:4123–4155

Christie I, Griffiths DF, Mitchell AR, Zienkiewicz OC (1976) Finite element methods for second order differential equations with significant first derivatives. Int J Numer Methods Eng 10:1389–1443

Celia MA, Binning P (1992) Two-phase unsaturated flow: one-dimensional simulation and air-phase velocities. Water Resour Res 28:2819–2828

Guarnaccia JF, Pinder GF (1997) NAPL: A mathematical model for the study of NAPL contamination in granular soils, equation development and simulator documentation. The University of Vermont, RCGRD #95–22

Kaluarachchi JJ, JC Parker (1989) An efficient finite elements method for modeling multiphase flow. Water Resour Res 25:43–54

Khoei AR, Mohammadnejad T (2011) Numerical modeling of multiphase fluid flow in deforming porous media: a comparison between two- and three-phase models for seismic analysis of earth and rockfill damps. Comput Geotech 38:142–166

Laplace PS (1806) Méchanique céleste, suppl. 10th vol

Mualem Y (1976) A new model for predicting the hydraulic conductivity of unsaturated porous media. Water Resour Res 12:513–522

Parker JC, Lenhard RJ, Kuppusamy T (1987a) A parametric model for constitutive properties governing multiphase flow in porous media. Water Resour Res 23(4):618–624

Parker JC, Lenhard RJ (1987b) A model for hysteretic constitutive relations governing multiphase flow 1. saturation-pressure relations. Water Resour Res 23(12):2187–2196

Suk H, Yeh GT (2007) 3D, three-phase flow simulations using the Lagrangian-Eulerian approach with adaptively zooming and peak/valley capturing scheme. J Hydrol Eng 12:14–32

Suk H, Yeh GT (2008) Multiphase flow modeling with general boundary conditions and automatic phase-configuration changes using a fractional-flow approach. Comput Geosci 12:541–571

Tsai CH, Yeh GT (2012) Retention characteristics for multiple-phasefluid systems, Terr Atmos Ocean Sci 23:451–458

van der Vorst HA (1992) Bi-CGSTAB: a fast and smoothly converging variant of Bi-CG for the solution of nonsymmetric linear systems. SIAM Sci Stat Comput 13:631–644

van Genuchten MTh (1980) A closed-form equation for predicting the hydraulic conductivity of unsaturated soils. Soil Sci Soc Am J 44:892–898

White MD, Oostrom M (1996) STOMP subsurface transport over multiple phases, Theory guide, PNL-11217. Pacific Northwest Laboratory, Richland, WA

Yeh GT, Fang YL, Zhang F, Sun JT, Li Y, Li MH, Siegel MD (2010) Numerical modeling of coupled fluid flow and thermal and reactive biogeochemical transport in porous and fractured media. Comput Geosci 14(1):149–170

Yeh GT, Tsai CH (2011) Proposing a new retention function for multiple phase-fluids. Abstract and Program, 2011 AGU Fall Meeting, CD, December 5–9, 2011